Coral Reefs (1990) 9:11–23

Coral Reefs

Gamma densitometry for the measurement of skeletal density

B. E. Chalker and D. J. Barnes

Australian Institute of Marine Science, P.M.B. No. 3, Townsville MC, Queensland 4810, Australia

Accepted 17 July 1989

Abstract. A method is described for the measurement of the density of calcium carbonate materials from the attenuation of a narrow, collimated beam of gamma photons. For the measurement of density for slices, approximately 0.5 to 1.0 cm thick, from the skeletons of reef building corals, the optimum beam energy is 30–34 keV; and measurement is practical from approximately 22 to 100 keV. The potential utilities of five commercially available isotopic sources (^{109}Cd, ^{125}I, ^{253}Gd, ^{210}Pb and ^{241}Am) are evaluated. Methods and results are presented for gamma densitometry using ^{210}Pb and ^{241}Am. The ^{210}Pb point source had its principal gamma emission at 46.5 keV. Bremsstrahlung and high energy (800 keV) gamma emissions associated with the ^{210}Pb decay granddaughter were detected, and procedures were developed to accommodate the contribution of these emissions to the overall count rate. The attenuation of count rate by aluminium and aragonite absorbers closely followed simple theoretical considerations provided that narrow energy window settings were used at the radiation monitor. These theoretical considerations take account of the density of the material absorbing the radiation, and hence the density could be determined from the attenuation of the gamma beam. Increased accuracy was achieved by the use of ^{241}Am and high speed counting equipment. ^{241}Am has its principal gamma emission at 59.6 keV. The attenuation of this gamma beam follows simple theoretical considerations for targets with mass thicknesses from 0 to 6 g cm^{-2}. Aragonite from the shell of a giant clam was found to have slightly different properties in the absorption of gamma photons to aragonite from a coral skeleton. The differences were small but statistically significant.

Introduction

Over the last two decades understanding of skeletal growth records has considerably expanded. A variety of environmental information can now be recognized in skeletal materials. In addition, demographic features of a population, such as growth rate, recruitment and survivorship, can also be determined from aspects of the records which are created during the growth of certain skeletal materials. The sorts of information which can be recognized in skeletal materials, and the uses to which such information can be put, are reviewed in Rhoads and Lutz (1980).

Certain massive reef corals have the potential to provide valuable records. This potential exists because of three features associated with skeletal growth in these corals. First, the growth rate is around 1–2 cm per year; and, consequently, any record included in the skeleton is resolvable at periods considerably shorter than a year. Second, these corals normally grow continuously; and the very large colonies occasionally found on most reefs can provide continuous records several centuries long. Third, seasonal variations in the density at which a skeleton is deposited provide a means by which any point in the skeleton can be dated (Knutson et al. 1972; Knutson and Buddemeier 1973; Hudson et al. 1976). The literature indicates that dating to periods in the order of 30–60 days should be relatively easy (e.g., Buddemeier 1974; Buddemeier and Kinzie 1975; Weber et al. 1975; Highsmith 1979; Wellington and Glynn 1983).

The causes of the annual density banding pattern in coral skeletons remain obscure, although the annual periodicity of the banding pattern has been established by several methods (Knutson et al. 1972; Moore and Krishnaswami 1972, 1974; Moore et al. 1973; Dodge and Thompson 1974; Dodge et al. 1974). The annual banding in coral skeletons almost certainly reflects seasonal changes in environmental conditions which alter the way in which corals add to their skeletons. Thus, the density patterns in coral skeletons may provide very long records of climate, and changes in climate, as well as providing the method by which this and other skeletal records can be dated.

The density banding patterns in coral skeletons were first seen in X-radiographs of slabs cut from the growth axes of massive skeletons (Knutson et al. 1972). Measure-

ments of the density variations associated with these banding patterns have been made by microdensitometry of such X-radiographs (Dodge and Thompson 1974; Buddemeier 1974; Buddemeier et al. 1974; Dodge and Brass 1984; Chalker et al. 1985). Microdensitometry of X-radiographs is convenient when the complete life span of a coral, or the period of interest, can be covered by a single X-radiograph, or by a couple of overlapping X-radiographs. Calibration of the procedures, and especially calibration for the non-uniform radiation characteristic of X-ray machines, makes extracting, standardizing and fitting together the data from several X-radiographs a difficult and tedious process. For example, using 24×30 cm X-ray plates, for which non-uniformity of the incident X-ray beam is manageable, 5 plates need to be exposed to cover a linear growth of 1 m (roughly 50–100 years of record), allowing about 30% overlap of the images on the plates. A minimum of 3 microdensitometer scans must be made along each plate: one for the image of the coral skeleton, and one each for the images of the secondary standards (aluminium bars) placed on either side of the area of interest in the skeleton (see Chalker et al. 1985). X-radiography has the advantage that it provides a "picture" of the density banding in coral skeletons. However, unless image analysis techniques are employed, data for skeletal density is obtained from a narrow microdensitometer track across the plate.

In theory, density could also be obtained by measuring the attenuation of a collimated beam of radiation (of approximately the same cross-sectional area as a microdensitometer light beam) as a slab of skeleton is moved across the beam. Such a system could have advantages over microdensitometry of X-radiographs in simplicity, accuracy, ease of calibration, and in obtaining density records for long sections (i.e., cores) of skeleton. It would have particular advantages in obtaining density records at the same time as scans are made for other records, for example, fluorescence records of terrestrial runoff (Isdale 1984).

This communication presents theory, procedures and results associated with measuring coral skeletal density using gamma densitometry. The discussion of theory includes the physics of gamma beam attenuation and the statistics of counting. The discussion of procedures includes practical considerations such as the selection of a radiation source, counting equipment and density standards. Optimization of these selections will depend primarily upon the nature of the samples (chemical composition, physical structure, thickness and density), the speed and accuracy required for density determination, and the availability and cost of the components. Results are presented for the measurement of the densities of a variety of standards with collimated beams of gamma photons from ^{210}Pb and ^{241}Am sources, which have their principal emissions at energies of 46.5 and 59.6 keV, respectively. This communication describes practical systems for measurements of coral skeletal densities by gamma densitometry. It also provides sufficient background information to simplify procedures for optimization of gamma densitometry techniques with other materials of equivalent mass thicknesses, such as mollusc shells.

Theory

Photon beam attenuation and the statistics of counting

The attenuation of a beam of gamma photons by a material is due both to outright absorption of photons and scattering out of the beam. When a monoenergetic beam is tightly collimated at both the source and the detector, attenuation is described by the equation

$$I = Io \exp(-\mu_1 \chi) , \quad (1)$$

where I is the intensity of the attenuated beam leaving the absorbing material (= transmitted beam), Io is the intensity of the incident beam, μ_1 is the linear absorption coefficient for the material, and χ is the thickness of the material. The value of μ_1 is a function of the energy of the incident gamma photons, the chemical composition of the absorbing material, and the density of the material. An alternative equation is

$$I = Io \exp(-\mu_m \varrho \chi) , \quad (2)$$

where μ_m is the mass absorption coefficient for the material and ϱ is its density. The value of the mass absorption coefficient (μ_m) is a function of the energy of the incident gamma photons and the chemical composition of the absorbing material. The product of density and thickness of the absorber ($\varrho\chi$) is known as the mass thickness.

Equation (2) can be rearranged to a form which is conveniently used for experimental determinations of mass absorption coefficients:

$$\ln(I) = \ln(Io) - \mu_m \varrho \chi . \quad (3)$$

Equation (3) provides that a plot of experimentally determined values of ln(I) against the mass thickness of an absorbing material should be linear and have a slope equal in magnitude but opposite in sign to the mass absorption coefficient.

When the radiation source provides multiple gamma emissions of different energies, the equations relating the intensities of the incident and transmitted beams become more complex. Equations describing the attenuation of gamma photon beams containing photons with two or three distinct energies are included in Appendix A. The use of these equations is discussed below. Appendix A also includes a brief description of "geometry" and "buildup", physical factors which must be considered in the construction of an operational counting system.

Density determination

When a beam of gamma photons is attenuated equally by a specimen material (sp) and a standard material (st) then,

$$\ln(Io/I)_{st} = \ln(Io/I)_{sp} = \mu_{mst} \varrho_{st} \chi_{st} = \mu_{msp} \varrho_{sp} \chi_{sp} \quad (4)$$

or

$$\varrho_{sp}=(\mu_{mst}/\mu_{msp})(\varrho_{st}\chi_{st})/\chi_{sp}\,. \tag{5}$$

When Eq. (5) is used to determine the density of a specimen material, values for μ_{mst} and μ_{msp} must be either calculated or measured. Values of μ_m for elements are published (Hubbell 1969; Bureau of Radiological Health 1970; Veigele 1973; Burr 1978). Values of μ_m for compounds and mixtures can be obtained from the equation

$$\mu_{mtotal}=\mu_{m1}\omega_1+\mu_{m2}\omega_2+\mu_{m3}\,\omega_3+\dots\,, \tag{6}$$

where ω_n is the mass fraction of a constituent element. Some particularly useful values of μ_m in the determination of the density of calcium carbonate skeleton are provided by Buddemeier (1974).

In the special case where the specimen material and the standard material have the same chemical composition then, because $\mu_{msp}=\mu_{mst}$, Eq. (5) simplifies to

$$\varrho_{sp}=(\varrho_{st}\chi_{st})/\chi_{sp}\,. \tag{7}$$

Materials and methods

Calculating mass attenuation coefficients

For each isotope under consideration, mass attenuation coefficients were calculated for four useful target materials: Al, $CaCO_3$, aragonite, and CaF_2. Aragonite was $CaCO_3$ which was assumed to contain 2% CH_2O and 0.8% Sr (Buddemeier 1974). For aluminium and for the constituent elements of the other targets, selected values of mass attenuation coefficients and gamma photon energies were obtained from Veigele (1973). For compounds, values at the tabulated gamma photon energies were calculated with Eq. (6).

All log-log plots of calculated mass attenuation coefficients vs. photon energies between 10 and 600 keV were initially linear and then curved and then became linear again. For all targets except Al, these curves were simulated with sixth order polynomials between 20 to 200 keV (polynomial regression, program P5R, BMDP Biomedical Computer Programs, Health Science Computing Facility, University of California, USA). Coefficients for polynomials greater than sixth order were not significant ($P>0.05$). For aluminium the polynomial was fitted from 20 to 150 keV. In all cases the polynomial fit was excellent ($r^2=1.00000$). The calculated mass attenuation coefficient for aragonite was used, as described in the next section, for the determination of optimum photon energies. The calculated mass attenuation coefficients for other target materials are supplied for comparison.

Determination of optimum photon energy

When skeletal density is determined by gamma densitometry it is necessary to make measurements of sufficient precision to detect small changes in density in a reasonably short counting time. This requirement limits the range of potential photon energies. If the photon energy is too high, almost all the photons will pass through the target; and small differences in absorption could not be detected without exceptionally long counting times. If the photons have an energy which is too low, they will almost all be absorbed; and small differences in absorption could not be distinguished from random variation in the background rate of counting without exceptionally long counting times. The optimal photon energy is a function primarily of the mass thickness and the mass attenuation coefficient, which is a function of the chemical composition, of the target.

An examination of the published literature shows that most reported values for the densities of scleractinian coral skeletons range from 0.8 to 2.0 g cm^{-3}, and that most X-radiographic studies have examined slices, approximately 0.7–0.8 cm thick, taken from the scleractinian skeletons. These values equate to mass thicknesses between 0.56 and 1.60 g cm^{-2}. In order to encompass the widest likely ranges in values, in the following sections we have considered optimum photon energies for measurements of 0.5 to 2.0 g cm^{-2}. In order to accommodate the more frequently observed range of values we have also considered mass thicknesses from 0.5 to 1.5 g cm^{-2}.

Estimates were made of measurement accuracies which would be expected using theoretical monoenergetic gamma photon sources with photon energies at 1 keV intervals between 22 and 100 keV. The target was a theoretical aragonite (see above). Calculations were made with the total number of photons striking the target material as 10^5, 10^6 and 10^7. At intervals of 0.01 g cm^{-2} for mass thicknesses between 0.50 and 2.00 g cm^{-2}, the number of photons (n) passing through the target material was calculated from Eq. (2) for the various photon energies and beam intensities. The 95% confidence limits were $n\pm1.96\,n^{1/2}$ (Wang 1969). Pairs of mass thicknesses corresponding to these confidence limits were calculated from the equation

$$\varrho\chi=\ln(I_0/I)/\mu m\,, \tag{8}$$

which was derived by the rearrangement of Eq. (3). The difference between each pair of determinations represented the width of the 95% confidence intervals ($CI\varrho\chi_{0.95}$) about the mass thicknesses.

The theoretical error, at a given level of probability, ($E\varrho\chi_p$) for a determination of mass thickness was defined as the width of the confidence interval about the true value of the mass thickness. For example at the 95% level of probability.

$$E\varrho\chi_{0.95}=CI\varrho\chi_{0.95}\,. \tag{9}$$

An alternative explanation of this relationship is that in 95% of all determinations the difference between the measured value of the mass thickness and the true value of the mass thickness would be less than one half of the $E\varrho\chi_{0.95}$.

The fractional error, at a given level of probability, ($F\varrho\chi_\varrho$) for a determination of mass thickness was defined as the theoretical error divided by the true value of the mass thickness. For example,

$$F\varrho\chi_{0.95}=E\varrho\chi_{0.95}/\varrho\chi\,. \tag{10}$$

In specific applications, each investigation must determine whether it is more appropriate to minimize the magnitude of the expected errors for the determinations of mass thicknesses, or to minimize the expected percentage errors. In the following sections of this contribution techniques are presented which enable either minimization.

For each combination of photon energy and beam intensity, the average width of the 95% confidence interval (i.e., the average error) was calculated,

$$AE\varrho\chi_{0.95}=\left(\sum_{\varrho\chi1}^{\varrho\chi2}CI\varrho\chi_{0.95}\right)\Big/(100(\varrho\chi2-\varrho\chi1)+1)\,, \tag{11}$$

where initially $\varrho\chi1=0.5$ g cm^{-2} and $\varrho\chi2=2.0$ g cm^{-2}.

Also calculated were the averages of the widths of the 95% confidence intervals divided by the true values of mass thickness (i.e., the average fractional errors),

$$AF\varrho\chi_{0.95}=\left(\sum_{\varrho\chi1}^{\varrho\chi2}CI\varrho\chi_{0.95}/\varrho\chi\right)\Big/(100(\varrho\chi2-\varrho\chi1)+1)\,. \tag{12}$$

Again, in the first instance, $\varrho\chi 1 = 0.5$ g cm^{-2} and $\varrho\chi 2 = 2.0$ g cm^{-2}. For the reasons, elaborated above, $AE\varrho\chi_{0.95}$ and $AF\varrho\chi_{0.95}$ were calculated again with mass thicknesses between 0.5 and 1.5 g cm^{-2}.

Because Eq. (8) is a log function, the confidence intervals were slightly asymmetric about the true mass thickness. Symmetric confidence intervals were calculated by an interactive procedure. First, the lower branch of the confidence interval about the true mass thickness was set equal to the higher branch; then the branches were progressively narrowed in width until they encompassed 95% of all determination for mass thickness. These calculations indicated that the asymmetry of the confidence intervals was so slight that it need not be considered further with regard to the results presented here.

Sources

Three types of sources are potentially for the determination of coral density from the attenuation of a beam of photons: X-ray machines, X-ray fluorescence sources and γ-emitting, isotopic sources. The use of X-ray machines is beyond the scope of this communication, although the principle discussed here would apply. X-ray fluorescence in the energy range of interest is typically produced by the excitation of a metal target with gamma photons from a ^{241}Am source. X-ray fluorescence would be attractive because a wide range of sources with discrete photon emissions are available. Unfortunately the intensities of such sources are not sufficient for the present application. Thus γ-emitting isotopic sources are considered here.

Seven potentially suitable isotopic sources are commercially available: ^{241}Am, ^{210}Pb, ^{153}Gd, ^{137}Cs, ^{133}Ba, ^{125}I and ^{109}Cd. These are listed in Table 1. ^{137}Cs and ^{133}Ba were eliminated from consideration because both emit moderately high energy photons (662 and 356 keV, respectively) as well as photons of energies suitable for gamma densitometry. The high energy photons associated with these sources would be inconvenient to shield.

Estimates were made for the measurement accuracies which could be achieved with the remaining five gamma sources. Counting rates at zero attenuation were measured for ^{241}Am and calculated for the other isotopes based upon the manufacturers' data for emissions and the efficiency of the detector at the relevant photon energy. A counting time of 16 s was selected for comparison because this enables overnight, automated counting of the samples normally processed in our laboratory. The target for comparison was again a theoretical aragonite (see above).

For each isotope, at mass thicknesses from 0.2 to 2.0 g cm^{-2}, the transmitted count rate was calculated from Eq. (2). From this the total number of counts accumulating over 16 s was calculated. Confidence intervals about the estimated mass thicknesses were calculated as previously described. The theoretical errors ($E\varrho\chi_{0.95}$) for the determinations of the mass thicknesses were calculated from Eq. (9); the fractional errors ($F\varrho\chi_{0.95}$) were calculated from Eq. (10).

Fabrication and characterization of density standards

Density standards were fabricated from four different types of material: aluminium, clam shell aragonite, coral skeleton aragonite and calcium fluoride.

A step-wedge was used as an aluminium density standard. The thickness of aluminium increased from 1.75 mm to 19.44 mm in 10 steps. Each step was about 14 mm deep, and the step-wedge was 20 mm wide. It was constructed of an alloy (Alcan 6063; 0.4% Si, 0.7% Mg) which had absorption coefficients for gamma radiation identical (within the limits of determination) with those listed for pure aluminium. This step-wedge was augmented with aluminium bars of similar chemical composition.

Eight aragonite standards were cut from the shell of the reef clam, *Tridacna gigas*. The standards were about 3 cm square and varied in thickness from 2.3 mm to 15.0 mm. Their densities were individually determined using the weight in air: weight in water method. Densities varied between 2.867 g cm^{-3} and 2.905 g cm^{-3}.

Coral aragonite standards were made from powdered coral skeleton. About 100 g of material was taken from a core of a large colony of *Porites lutea*. The material was selected without regard for density banding, except that it would have included pieces from several different bands. It was powdered with an agate vibrating cup mill (Humbolt Wedag, Köln, Federal Republic of Germany), initially for 5 min and then for 6 periods each of 3 min. The interruptions were to prevent overheating of the mill and of the skeletal material. The powder was dried at 50° C overnight. Particle sizes were determined with a Coulter counter. All particles were smaller than 50 μm; 95% of them were smaller than 32 μm, and 50% were in the range 10–16 μm. Portions of the powder were pressed into solid plugs using a stainless steel piston, 19.40 mm in diameter, which exactly fitted into a stainless steel cylinder with a depth of about 1.5 cm. The cylinder was loaded with powder and a hydraulic press was used to apply 20 tonnes overall pressure to the piston. The resulting plug of skeletal material was carefully pressed from the cylinder, and it remained intact provided it was handled gently. Different amounts of powder were loaded into the cylinder and, in this way, provided 7 plugs of diameter 19.40 mm varying in thickness from 1.53 mm to 7.42 mm. The plugs were weighed and, since their volume could be calculated from their dimensions, their density could be determined. Densities ranged between 2.359 g cm^{-3} and 2.424 g cm^{-3}, with an average value of 2.407 g cm^{-3}.

A set of coral skeletal slices were used to confirm the efficacy of densitometry techniques. These specimens were constructed from a 100 mm diameter core drilled vertically from a large colony of *Porites lutea*. The core was cut horizontally, that is, parallel to the annual density bands, into 4.7, 6.9, 10.2, 12.4 and 15.0 mm thick slices. The average density of each slice was determined by weighing and calculating its volume from the measured dimensions of the slices. The slices were exposed to the ^{241}Am gamma beam at 5 positions equidistant across the diameter of the slice.

Table 1. Summary table of commercially available low energy X-ray and gamma photon sources and calculated mass attenuation coefficients for commonly used target materials

Isotope	Photon emission (keV)	Activity of commercial source (GBq)	Photons s^{-1} steradian^{-1}	Half-life	Mass attenuation coefficients (cm^2 g^{-1})			
					Al	$CaCO_3$	($CaCO_3$ + 2%CH_2O + 0.8% Sr)	CaF_2
^{241}Am	59.6	3.7	2.2×10^7	433 y	0.281	0.377	0.396	0.433
^{210}Pb	46.5	0.74	1.4×10^6	20.4 y	0.420	0.613	0.651	0.734
^{153}Gd	41.3 (Eu K_α X-rays)	37	1.0×10^9	241.5 d	0.530	0.802	0.855	0.975
^{137}Cs	32.1 (Ba K_α X-rays)	11.1	–	30.17 y	0.945	1.50	1.61	1.87
^{133}Ba	30.9 (Cs K_α X-rays)	0.37	–	10.8 y	1.04	1.66	1.78	2.08
^{125}I	27.4 (Te K_α X-rays)	18.5	1.2×10^9	60.6 d	1.42	2.29	2.46	2.88
^{109}Cd	22.1 (Ag K_α X-rays)	0.74	5.0×10^7	462 d	2.57	4.16	4.45	5.27

A set of calcium fluoride standards was created from 2 mm thick disks of CaF_2 (Part No. 7000-378, Spectra-tech, Inc., Stanford, Connecticut, USA) by stacking the disks to thickness of CaF_2 between 2 and 8 mm. Such disks are supplied as end-windows for sample holders used in IR spectrophotometers.

Count rates were plotted against mass thickness for the various density standards using different window settings for two densitometry systems (^{210}Pb and ^{241}Am; see Appendix B). The curves were either modelled by equation (3) (^{241}Am system) and fitted by linear regression analysis or modelled by equations (3, A1 and A2) (^{210}Pb system) and fitted by non-linear least-squares regression analysis (program P3R, BMDP Biomedical Computer Programs, Health Science Computing Facility, University of California, USA).

Results

Determination of optimum photon energy

The theoretical accuracy for the determination of mass thickness between 0.5 and 2.0 g cm^{-2} (i.e., values appropriate to coral density work) with photon energies between 22 and 100 keV are shown in Fig. 1. The average width of the 95% confidence intervals about the mass thickness determinations ($AE\varrho\chi_{0.95}$) are plotted vs. photon energy. Regardless of the total number of incident photons (between 10^5 and 10^7), the narrowest 95% confidence intervals occur when the energy of the gamma photons is 33 keV. When the data were plotted for the average fractional errors ($AF\varrho\chi_{0.95}$), the optimum gamma energy was 32 keV.

If a range of samples of lower average mass thickness is to be measured, the optimum photon energy would be lower. For example, when mass thicknesses ranged between 0.5 and 1.5 g cm^{-2}, the optimum photon energy was 30 keV. In this case optimum energy applies to both minimization of average error and average fractional error.

The results demonstrate that the range of photon energies practical in gamma densitometry of coral samples is about 24 to 60 keV. It would not normally be practical to use a beam of photons with energies less than 22 keV because the photons would be substantially absorbed at mass thicknesses in excess of 1.7 g cm^{-2}. Between 60 and 100 keV, the width of the 95% confidence intervals about a measurement increases almost in direct proportion to energy. The rise is particularly great when the total number of counts accumulated is 10^5 or less.

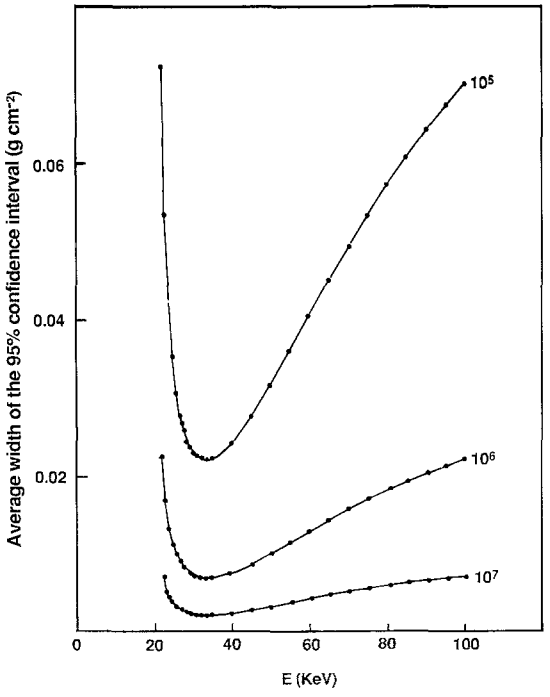

Fig. 1. Average width of the 95% confidence intervals for determinations of mass thickness (0.5 to 2.0 g cm^{-2}) vs. photon energy from 22 to 100 keV. The total number of incident photons are 10^5, 10^6 and 10^7 respectively. The target is theoretical biogenic carbonate (calcium carbonate with 2% organic matter and 0.8% strontium)

Source evaluation

Figure 2 illustrates the accuracies of mass thickness measurements between 0.5 and 2.0 g cm^{-2} which would be expected using ^{241}Am, ^{210}Pb, ^{153}Gd, ^{125}I and ^{109}Cd as photon sources. The width of the 95% confidence intervals about determinations of mass thickness ($CI\varrho\chi_{0.95} = E\varrho\chi_{0.95}$) are plotted vs. the actual mass thickness. In all cases the magnitude of the theoretical error ($E\varrho\chi_{0.95}$) increases with increasing mass thickness.

Some investigators may wish to select a source so as to minimize fractional errors of measurement. Given an optimal photon energy of 32–33 keV (see above) and mass thicknesses in the range 0.5–2.0 g cm^{-2}, isotopes with photon energies which are less than optimal (e.g., ^{109}Cd) give results for which the fractional error ($F\varrho\chi_{0.95}$) increases with increasing mass thickness. Isotopes with photon energies which are greater than optimal (e.g., ^{153}Gd, ^{210}Pb, ^{241}Am) give results for which the fractional error decreases with increasing mass thickness. ^{125}I has a photon energy which is close to optimal and the fractional error does not much change over this range of mass thicknesses. Figure 2 illustrates these results.

Characterization of sources and their use in gamma densitometry

The energy spectrum of the ^{210}Pb gamma source (Fig. 3), measured with the Eberline-Bertold system (Appendix B), showed two distinct peaks. The photon energies associated with both peaks were estimated from their mass absorption coefficients (Bureau of Radiological Health 1970; Buddemeier 1974) and found to be approximately 46.5 keV. This strongly indicated that the larger peak was the 46.5 keV gamma emission characteristic of ^{210}Pb, and the smaller peak was due to Compton scatter caused by the 46.5 keV ^{210}Pb emission. The discrepancy between the experimentally determined energy for the photons in the smaller peak and its displacement to the left in the energy spectrum (Fig. 3) indicated that the Compton scatter occurred chiefly in the end window of the scintillation probe. That is, the smaller peak was due to 46.5 keV

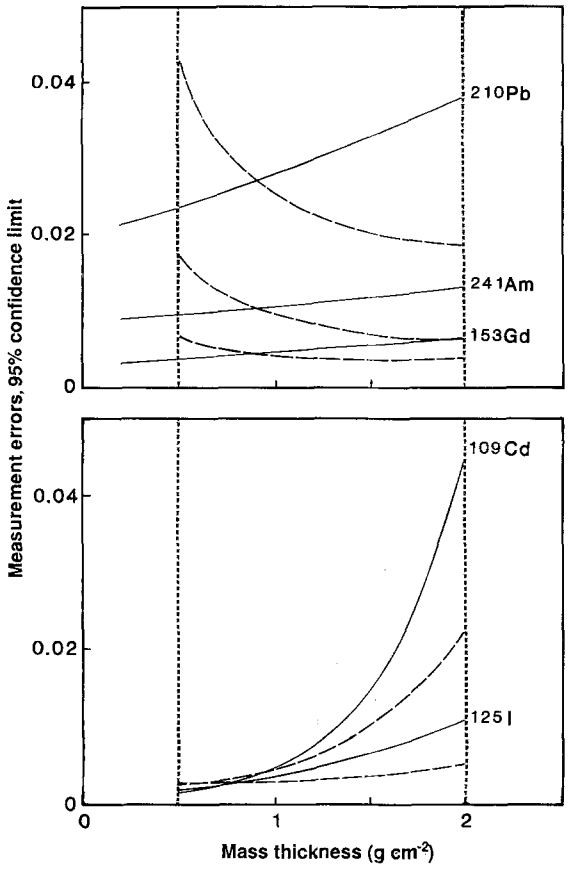

Fig. 2. Measurement errors: (1) theoretical errors (solid curves), (widths of the 95% confidence intervals, g cm^{-2}) vs. mass thickness for five commercially available gamma sources. Based upon counting statistics only, 95% of the time the magnitude of the error in the determination of the mass thickness will be no greater than half the value shown. (2) Fractional errors (dashed curves, which on the right side of the figure are located directly below the solid curves representing theoretical errors for the same isotopes) (widths of the 95% confidence intervals divided by the true values of mass thickness) vs. mass thickness. The density measurements are based upon a 2 mm diameter beam collimated over 4 cm. The activity is taken from commercial specifications. The counting time is 16 s. The target is theoretical biogenic carbonate (calcium carbonate with 2% organic matter and 0.8% strontium)

photons which passed into the target and then gave rise to lower energy emissions when they collided with materials in the probe. The "tail" to the right of the main peak (Fig. 3) was Bremsstrahlung radiation caused by high energy beta emissions from the source. The low energy radiation monitor could not detect the high energy peak at about 800 keV which would have been caused by gamma emissions from the ^{210}Po decay granddaughter of ^{210}Pb. These gamma photons had sufficient energy to penetrate the lead shielding used to collimate lower energy gamma emissions, and some would have been detected by the low energy gamma probe because of Compton scatter which would produce emissions within the energy range to which the monitor was sensitive. The lack of very low energy emissions in Fig. 3 indicated that the Bi L X-rays (9.42–16.4 keV) characteristic of the ^{210}Pb source were absorbed within the source and by the surrounding capsule.

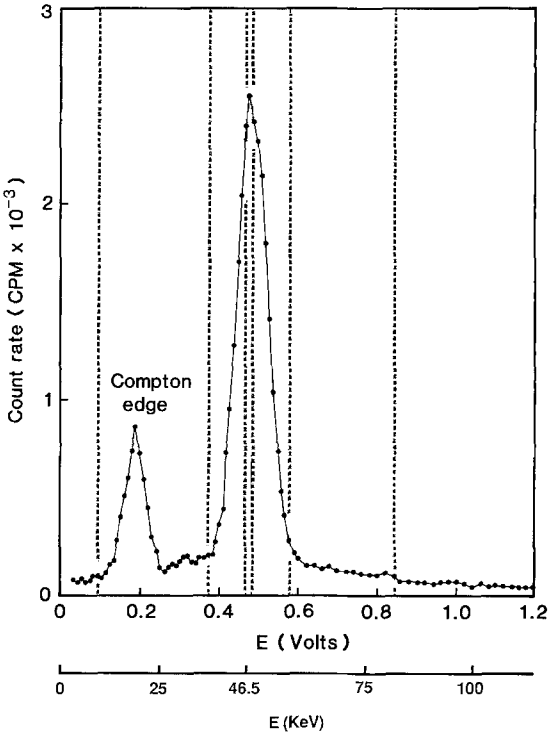

Fig. 3. Energy distribution for a collimated beam of ^{210}Pb gamma photons showing amplifier voltage versus count rate. The photomultiplier voltage was 1200 V. The spectrum was generated with the amplifier window width set at 10 mV, this window is indicated by the closely spaced pair of lines at the centre of the main peak (46.5 keV) which occurred at 480 mV. The more widely spaced pairs of lines indicate window widths of 200 and 500 mV

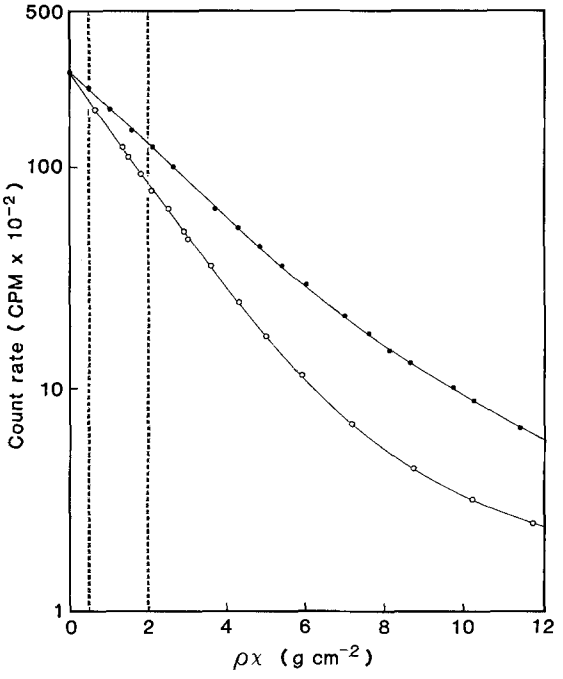

Fig. 4. Extended data sets illustrating count rate versus mass thickness. The target materials were aluminium (closed circles), and clam aragonite (open circles). The photomultiplier voltage was 1196 V; amplifier voltage (E) was 480 mV; ΔE was 200 mV. Vertical lines mark the region relevant to the routine determination of coral skeletal densities

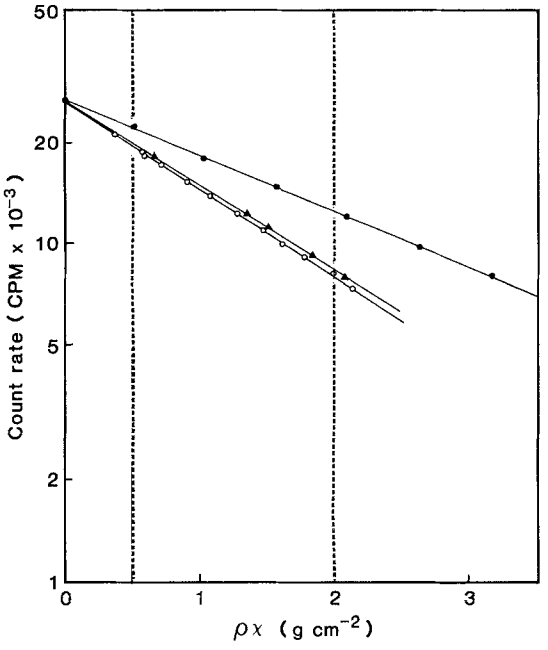

Fig. 5. Truncated data sets illustrating count rate versus mass thickness. The target materials were aluminium (closed circles), clam aragonite (closed triangles) and pellets pressed from powdered coral aragonite (open circles). Detector settings were the same as those used in Fig. 4. Vertical lines mark the region relevant to the routine determination of coral skeletal densities

Figure 4 exemplifies mass attenuation curves; specifically, it illustrates how different mass thicknesses of clam aragonite and aluminium attenuated the ^{210}Pb count rate. Attenuation was initially log-linear and then curved significantly at greater mass thicknesses. Figure 5 is a detailed example of mass attenuation curves over the range of mass thicknesses which are likely to be encountered during density measurements of sections from coral skeletons. Attenuation was log-linear. These curves and others were mathematically described by equations selected from among Eqs. (3), (A2), (A1) and (A4). Parameter values, which are obtained when experimental data is fitted with these equations, are presented in the following tables.

Tables 2 and 3 contain the parameters for the equations which mathematically describe the attenuation of the ^{210}Pb beam by three different materials: powdered coral aragonite, clam shell, and aluminium. For each target material a mass attenuation curve was constructed for each of four detector window settings. Data collected from relatively narrow window settings is presented in Table 2. The detector window for the top half of Table 2 was 475–485 mV, and the detector window setting for the bottom half of Table 2 was 380–580 mV. Data collected from relatively wide window settings is presented in Table 3. The top half of the table presents data collected with a window between 100 and 600 mV. The bottom half of the table presents data describing mass attenuation curves constructed with the monitor set in integral mode (E > 100, see Appendix B).

For all complete data sets, the mass attenuation curves were modelled with Eqs. (A2) (3 parameters: Io_1, μm_1, and Io_2) and (A1) (4 parameters: Io_1, μm_1, Io_2 and μm_2). The values of these parameters and the confidence intervals about each determination are presented in the tables, when the parameter values are statistically significant ($P < 0.05$).

Tables 2 and 3 also present the values of the parameters describing data sets that were truncated to include only values falling within the range of mass thickness appropriate to measurement of density in coral skeletons. For biogenic aragonite this includes mass thicknesses up to 2.15 g cm^{-2}. Because aluminium has a lower mass attenuation coefficient, greater mass thickness are required to achieve equivalent beam absorption; and for the aluminium standards, the truncated data included mass thickness up to 3.18 g cm^{-2}. When both standards are measured using the isotope ^{210}Pb this is equivalent to values of $0 \leqq \mu_1 \chi = \mu_m \varrho \chi \leqq 1.3$. For the truncated data sets, the mass attenuation curves were modelled with Eqs.

Table 2. Summary table of values for Io_1, Io_2 (when statistically significant, $P < 0.05$) and the respective mass attenuation coefficients for various materials using a collimated ^{210}Pb gamma photon beam. The model Eqs. were (3), (A3) and (A2) for models of two, three, and four parameters respectively

Material	ΔE (mV)	$\varrho\chi$ (g cm^{-2})	Io_1 (cpm)	95% CI	μm_1 (cm^2 g^{-1})	95% CI	Io_2 (cpm)	95% CI	μm_2 (cm^2 g^{-1})	95% CI	r^2	n	Eq.
Coral (powdered)	475–485	0– 1.79	2627	± 23	0.6031	±0.0091	–	–	–	–	0.9998	8	(3)
Clam		2.08	2630	± 39	0.5795	±0.0094	–	–	–	–	0.9999	6	(3)
		7.19	2633	± 48	0.5864	±0.0087	11.63	± 2.81	–	–	0.9999	14	(A2)
Aluminium		0– 3.18	2664	± 49	0.3939	±0.0100	–	–	–	–	0.9995	7	(3)
		0– 5.39	2625	± 51	0.4051	±0.0218	41.85	± 40.47	–	–	0.9996	11	(A2)
Coral (powdered)	380–580	0– 2.15	26560	±250	0.5996	±0.0073	–	–	–	–	0.9997	13	(3)
		0– 3.07	26240	±210	0.6173	±0.0156	400.1	± 202.5	–	–	0.9998	17	(A2)
Clam		0– 2.08	26910	±360	0.5834	±0.0095	–	–	–	–	0.9999	6	(3)
		0– 7.19	27810	±460	0.5848	±0.0083	364.2	± 33.1	–	–	0.9996	14	(A2)
Aluminium		0– 3.18	27030	±320	0.3862	±0.0063	–	–	–	–	0.9998	7	(3)
		0–11.36	26320	±500	0.3881	±0.0061	368.4	± 32.5	–	–	0.9998	19	(A2)
		0–11.36	25470	±910	0.4182	±0.0185	1746	±1072	0.1192	±0.0455	0.9999	19	(A1)

(3) (two parameters: Io_1 and μm_1), and Eqs. (A2) and (A1). Again the parameter values are presented in the tables only when the values are statistically significant ($P<0.05$).

Results presented in Table 2 demonstrate that when mass attenuation curves are determined for any of the three target materials with ^{210}Pb, narrow detector windows, and relatively large mass thicknesses, the curves can be effectively modelled with either Eqs. (A2) or (A1) ($r^2>0.9996$). For the smaller range of mass thicknesses encountered during the measurement of skeletal densities in coral cores, the curves become log-linear and must be modelled with Eq. (3) ($r^2>0.9995$).

When mass attenuation curves were constructed with wide detector windows, such as those used to produce the data contained in Table 3, the situation became more complex. When a detector window width of 500 mV was used, graphs of count rate (^{210}Pb) vs. mass thickness showed additional curvature at small values of mass thickness. This was due to relatively low energy Bremsstrahlung radiation and to low energy gamma photons being counted in a higher energy window due to coincidence. The curves could be modelled effectively with Eq. (A4); however determination of accurate parameter values required an inconveniently large number of measurements. This problem was eliminated by interposing an aluminium filter between the source and the target. This filter was 0.82 mm thick, and it removed essentially all of the very low energy gamma photons. The resultant attenuation curves produced with the filtered beam, could be effectively modelled by Eqs. (A1) and (A2); and the corresponding values for the parameters in these equations are shown in the top half of Table 3.

The data presented above were obtained with the monitor used as a pulse height analyser. With narrow window settings in this mode, small deviations of the photomultiplier voltage from its optimum setting could cause large deviations in the observed count rate. It was possible to set the monitor so that only events above selected energy were counted. This alternative setting, with $E>100$ mV (see Appendix B), produced a plateau for count rate versus photomultiplier voltage. Attenuation curves produced with these settings could be effectively modelled with Eq. (A4). Using the wide window technique described above, the beam was filtered with a 0.82 mm thick aluminium plate; and the resultant attenuation curves were modelled with Eqs. (A2) and (A1). Values for the relevant parameters for both complete and truncated ($0\leqq\mu_m\varrho\chi<1.3$) data sets are listed in the bottom half of Table 3.

The energy spectrum of the ^{241}Am gamma source (Fig. 6) measured with the Canberra Packard System (Appendix B) showed three distinct peaks. There was a primary peak at 59.6 keV, a peak mainly due to Compton scatter but which would also have contained contributions from gamma photons at 26, 33 and 43 keV, and a third peak due to Np L X-rays (12–22 keV).

Table 4 describes the attenuation of the ^{241}Am beam by different thicknesses of five materials: powdered coral aragonite, slices from coral cores, clam shell, aluminium, and calcium fluoride. The upper half of the table describes mass attenuation curves obtained with a detector window set with a width of 200 mV (220–420 mV). The lower half of the table describes mass attenuation curves constructed with the monitor set in the integral mode ($E>220$, see Appendix B). In all cases the mass attenu-

Table 3. Summary of parameter values (when statistically significant, $P<0.05$) modelling attenuation curves for various materials intercepting a collimated ^{210}Pb gamma photon beam. The model Eqs. were (3), (A3) and (A2) for models of two, three, and four parameters respectively

Material	ΔE (mV)	$\varrho\chi$ ($g\,cm^{-2}$)	Io_1 (cpm)	95% CI	μm_1 ($cm^2\,g^{-1}$)	95% CI	Io_2 (cpm)	95% CI	μm_2 ($cm^2\,g^{-1}$)	95% CI	r^2	n	Eq.
Coral	100–600	0– 2.15	33290	± 430	0.5420	±0.0098	–	–	–	–	0.9993	13	(3)
(pow-		0– 2.15	31510	± 490	0.6277	±0.0265	2372	± 627	–	–	0.9999	13	(A2)
dered)		0– 3.07	31730	± 160	0.6145	±0.0104	2059	± 172	–	–	0.9999	17	(A2)
Clam		0– 2.08	33890	± 540	0.5348	±0.0111	–	–	–	–	0.9998	6	(3)
		0– 2.08	32580	± 820	0.5823	±0.0316	1521	± 919	–	–	1.0000	6	(A3)
		0–11.70	31010	±1570	0.5185	±0.0205	1030	± 71	–	–	0.9988	17	(A3)
		0–11.70	31250	± 620	0.5860	±0.0182	2536	± 405	0.0807	±0.01456	0.9999	17	(A2)
Aluminium		0– 3.18	33870	± 620	0.3535	±0.0097	–	–	–	–	0.9994	7	(3)
		0– 3.18	32270	±1630	0.3945	±0.0458	1920	±1897	–	–	0.9998	7	(A3)
		0–11.36	31820	±1040	0.3660	±0.0127	1424	± 124	–	–	0.9992	19	(A3)
		0–11.36	28850	±1660	0.4392	±0.0326	5596	±1918	0.1084	±0.02750	0.9998	19	(A2)
Coral	>100	0– 2.15	30690	± 440	0.4879	±0.0110	–	–	–	–	0.9988	13	(3)
(pow-		0– 2.15	28150	± 440	0.5995	±0.0239	3190	± 551	–	–	0.9999	13	(A3)
dered)		0– 3.07	28150	± 150	0.6010	±0.0104	3209	± 165	–	–	0.9999	17	(A3)
Clam		0– 2.08	31060	± 750	0.4836	±0.0168	–	–	–	–	0.9994	6	(3)
		0– 2.08	28760	±1090	0.5645	±0.0442	2600	±1204	–	–	1.0000	6	(A3)
		0–11.70	26700	±2720	0.4659	±0.0471	1972	± 252	–	–	0.9929	17	(A3)
		0–11.70	25370	±2250	0.6367	±0.0941	6109	±1933	0.1028	±0.0308	0.9979	17	(A2)
Aluminium		0– 3.18	31800	±1860	0.3252	±0.0315	–	–	–	–	0.9929	7	(3)
		0–11.36	29440	± 850	0.3586	±0.0125	2184	± 133	–	–	0.9992	19	(A3)
		0–11.36	28180	±1750	0.3937	±0.0403	3978	±2048	0.04842	±0.04175	0.9994	19	(A2)

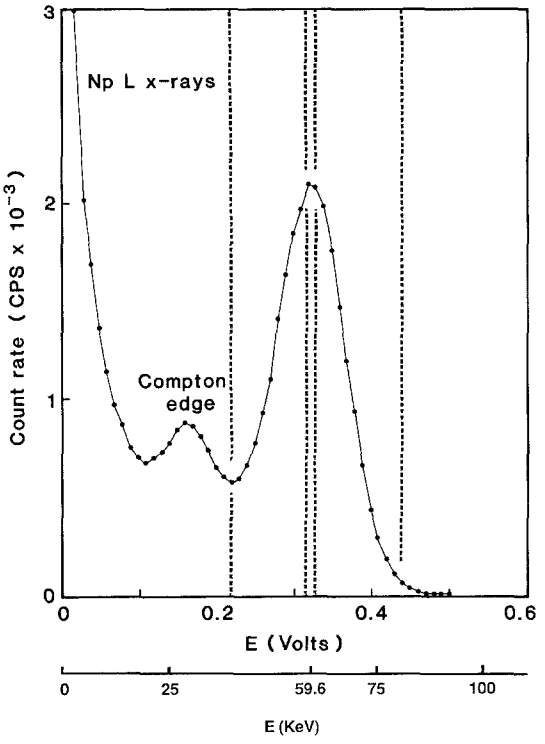

Fig. 6. Energy distribution for a collimated beam of ^{241}Am gamma photons showing amplifier voltage versus count rate. The photomultiplier voltage is 1420 V. The amplifier window width was set at 10 mV, and this window width is indicated by the closely spaced pair of lines at the centre of the main peak which occurred at 325 mV. The more widely spaced pair of lines indicates a window width of 200 mV

ation curves were log-linear over the range of mass thickness which was examined, and the curves were effectively modelled with Eq. (3). For sections from coral cores, the coefficients of determination (r^2) were 0.9991 and 0.99995; in all other cases the coefficients of determination were 0.99999 or greater. Variations in the initial count rates (Io_1) were due primarily to differences in the alignment of the photon beam.

Discussion

Optimum photon energy

The optimum photon energy for gamma densitometry depends primarily upon the mass thickness and chemical composition of the target material. For aragonite with mass thicknesses between 0.5 and 1.5 g cm^{-2}, the optimum photon energy is 30 keV; and for mass thicknesses between 0.5 and 2.0 g cm^{-2}, the optimum energy is 32–33 keV. Previously, most automated measurement of coral skeletal density have been made by densitometry of X-radiographs. The optima reported here can not be directly compared to standard practice in X-radiography of coral skeletal slices because X-ray machines emit photons with a broad distribution of energies. However, in general, equivalent beam attenuation is produced when the energy of an X-ray beam measured in kVp is approximately 1.5 times the energy of a gamma photon beam measured in keV (Buddemeier 1974). Most publications involving X-radiography of coral skeletal slices report the use of beam energies between 45 and 52 kVp, which is equivalent to photon sources of energies in the range 30–35 keV.

Selection of a source and counting equipment

The selection of a source and counting equipment for gamma densitometry will be influenced by a variety of considerations. Standardization is simplified if the isotope has a single emission in the energy region of the interest. Shielding problems are minimized if the isotope and its decay products do not have significant high energy emissions. The isotope must be available at a suitably high specific activity, and it should have a half-life long enough for convenient and accurate counting. Optimally it should be readily available in a physically convenient sealed source and at a low cost.

Seven isotopes with potentially suitable energies, half-lives, and activities are commercially available (Table 1).

Table 4. Summary of parameter values; attenuation curves for various materials intercepting a collimated ^{241}Am gamma photon beam are modelled with Eq. (3)

Material	ΔE (mV)	$\varrho\chi$ (g cm^{-2})	Io_1 (cps)	95% CI	μ_{m1} (cm^2 g^{-1})	95% CI	r^2	n
Coral (powdered)	220–240	0–5.99	15299	± 7	0.38081	±0.00015	1.00000	19
Coral (core)		0–5.53	15541	±107	0.40018	±0.00226	0.99991	13
Clam		0–5.89	15409	± 1	0.37211	±0.00002	1.00000	12
Aluminium		0–5.39	15591	± 28	0.27747	±0.00055	0.99999	11
CaF_2		0–2.61	15690	± 44	0.43081	±0.00172	0.99999	5
Coral (powdered)	>220	0–5.99	15608	± 9	0.38227	±0.00017	1.00000	19
Coral (core)		0–5.53	15430	± 80	0.39000	±0.00170	0.99995	13
Clam		0–5.89	15758	± 35	0.37358	±0.00070	0.99999	14
Alumunium		0–5.39	15918	± 13	0.27909	±0.00025	1.00000	11
CaF_2		0–2.61	15580	± 7	0.42391	±0.00027	1.00000	5

^{137}Cs and ^{133}Ba were previously eliminated from consideration because both emit moderately high energy photons which would be inconvenient to shield. In addition, the specific activity of ^{133}Ba is low relative to that of other, more convenient, isotopes.

The final selection of source and counting equipment will, in most cases, be influenced by the following considerations: (1) the funds available for the initial purchase of the system; (2) funds available for the replacement of the source as it decays; (3) the accuracy required; (4) the length of time available to make the measurements. This communication has demonstrated that using relatively low speed counting equipment (count rate $\leqq$40 000 cpm) coral skeletal densities can be accurately measured using the isotope ^{210}Pb. However, because of the relatively low activity of this isotope (Table 1), counting times of 2 minutes for each measurement are required in order to achieve an accuracy of 2.7% ($F\varrho\chi_{0.95}$, $\varrho\chi=1.0$). With the acquisition of high speed counting equipment (40 000 cpm $\leqq$ count rate $\leqq$ 40 000 cps), increased accuracy and shorter counting times can be achieved with the isotope ^{241}Am. Three other isotopes deserve special consideration: ^{153}Gd, ^{125}I and ^{109}Cd. The measurement errors (95% confidence limits) which would be expected when measuring coral density with all of these isotopes is illustrated in Fig. 2.

Use of high speed counting equipment and the isotope ^{109}Cd to measure coral density, would result in errors limits (95%) ranging from 0.3 to 2.6% for mass thickness from 0.5 to 2 g cm^{-2}. Because the Ag Kg X-rays from ^{109}Cd have an energy of only 22.1 keV, this isotope provides greater accuracies at lower mass thickness; and lower accuracy at greater mass thickness when most of the photons have been absorbed. The greatest counting accuracies can be produced using the remaining two isotopes: ^{153}Gd and ^{125}I. These isotopes are both available at extremely high specific activities. In constructing Fig. 2, the initial count rates were limited to 40 000 cps; and this resulted in errors of 0.6% or less (95% CI) for mass thickness from 0.5 to 2 g cm^{-2}. If very high speed counting equipment (such as gated amplifiers) are available, larger initial count rates may be used and smaller measurement errors can be achieved.

In summary, high speed counting equipment is required in order to achieve reasonable accuracy in a short time. The isotope ^{241}Am appears to be sufficiently accurate for most measurements; and, because of its long half-life, frequent source replacement and counting time compensation for decay are not required. Increased accuracy can be achieved with ^{153}Gd; but this is the most expensive of the isotopes listed in Table 1, and because it has a half-life of 241.5 days, periodic replacements would be required. ^{125}I is more inconvenient, because it has a half-life of only 60.0 days which necessitates frequent replacement of the source. In addition some consideration must be given to the presence within the ^{125}I source of small amounts of ^{126}I which, in addition to Te K X-rays, emits X-rays at 386 and 667 keV. However, ^{125}I could be used for highly accurate measurements, particularly for mass thicknesses between 0.5 and 1.0 g cm^{-2}.

Density standards and measurements

When measuring coral skeletal density, the most appropriate primary standard is a portion of the target coral skeleton, which has been powdered and pressed into plugs. These plugs can be used to construct mass attenuation curves; which, in the experimental region of interest, are modelled by Eqs. (1)–(3). Provided that sufficient skill is exercised in fabrication and the plugs are counted long enough, extremely high accuracies can be achieved ($r^2=1.00000$). Coral powder pellets are, however, fragile. If the respective mass attenuation coefficients have been measured, the coral powder pellet primary standards can be replaced in routine operations by secondary standards such as clam aragonite or aluminium. These materials can be machined to form step or continuous wedges. Standards of fixed geometry have special advantages in automated densitometry techniques. One difficulty is that these materials may vary in chemical composition when obtained from different sources. Aluminium metal suitable for machining into standard sets is sometimes an alloy of uncertain chemical composition. We have eliminated this problem by the adoption of high purity, crystalline calcium fluoride as our secondary standard. Standard sets can be constructed by stacking 2 mm thick disks which are used as sample carriers for IR spectrophotometers. Mass attenuation curves for these calcium fluoride disks are log-linear (r^2 = 0.99999) from mass thickness of zero to at least 2.6 g cm^{-2}, which is much in excess of the range required during the routine measurement of coral skeletal densities.

It is a physical necessity that mass attenuation curves for coral skeletons and powder plugs made from them are, on average, identical. Variations in mass attenuation coefficients for corals collected from different locations may be anticipated and must be considered in the selection of primary and secondary density standards. This variation is illustrated by comparing mass attenuation coefficients for the coral powder plugs and slices from coral cores, as listed in Table 4. It is to be expected that the core sections will show slightly higher variability than the powder plugs, because the coral density bands within the coral core sections are not exactly parallel and are not uniform from year to year. Indeed if uniformity were anticipated there would be little practical reason for developing the techniques which are described here. The mass attenuation curves for the slices of coral cores confirm that gamma densitometry can be used effectively for the measurements of the density of sections of coral skeletons.

The small, but statistically significant, difference in the attenuation of gamma photons between coral aragonite and clam aragonite (Tables 2–4) was probably due to slight differences in the inorganic and organic inclusions (see Buddemeier 1974). Results presented here indicate that if clam shell were used as the primary aragonite standard in measurements of coral skeletal density then the measured densities would be about 1.5–2.0% lower than the true densities. Of course, count rates must be high enough, or count times long enough, before this difference becomes significant. The difference between clam

and coral aragonite suggests that small variations in apparent skeletal density of corals could arise because of differences in chemical composition within and between colonies of one species, between collection sites, and between species. Surveys to test for such effects would have to be made before very accurate coral skeletal density measurements became appropriate. Such surveys would be most easily made with techniques described here, but could also be made with X-radiography techniques after appropriate calibration (Chalker et al. 1985).

Summary

This communication has explored theoretical and practical considerations relevant to the use of a sealed source of gamma radiation in the measurement of coral skeletal density. Measurement of coral skeletal density by gamma densitometry first requires calibration of the instrumentation. The simplest situation occurs when the standards used for calibration have, or are assumed to have, the same chemical composition as the skeletal material to be measured. These standards are used to determine how count rate varies with density and thickness. Variation in count rate is related to density and thickness by the mass attenuation coefficient. Thus, the first step in the procedure is the construction of standard curves of the sort illustrated by Fig. 5, and the determination of the mass attenuation coefficients using Eq. (3). Mass attenuation coefficients may also be obtained from tabulated values, if available. Once the relationship between count rate and mass thickness has been established, skeletal density can be determined using Eq. (7) from the count rate of the gamma beam after it has passed through a known thickness of skeletal material.

Plugs of powdered coral skeleton are the most appropriate standards for coral densitometry. Such plugs are delicate; and, in practice, it may be more convenient to use a secondary standard made from a different material. Where secondary standards are used, the count rate of the gamma beam after it has passed through a known thickness of coral skeleton is related via Eq. (3) to the mass thickness of the secondary standard which would produce the same attenuation. The mass attenuation coefficient of the secondary standard may be obtained from the calibration curve; the mass attenuation coefficient of coral skeleton may be calculated (e.g., Buddemeier 1974) or determined using plugs of powdered skeleton; and the density of the coral skeleton can then be calculated using Eq. (5).

Gamma densitometry of coral skeletons is quicker, simpler and subject to fewer sources of variability than measurement of coral skeletal density from optical densitometry of X-radiographs, but it requires construction of specialized equipment whereas optical densitometry of X-radiographs utilizes standard laboratory and medical equipment. The greatest utility of gamma densitometry will probably be in the analysis of long cores drilled from large coral colonies, or in situations where high accuracy and precision are required.

Acknowledgements. We thank Mr. R. Barnes, Mr. M. Devereux, Mr. E. Daniel, Mr. A. Saunders and Ms. J. Wu Won for skilled technical assistance. Mr. E. Gill kindly assisted with the electronics associated with the radiation monitor. Professor R. Taylor (James Cook University of North Queensland) and Dr. P. Burnes, Dr. L. Martin and Mr. J. Mika (Australian Radiation Laboratory) provided very useful advice regarding the emissions associated with the source and the responses of the radiation monitor. Dr. P. Isdale and Mr. E. Daniel collected the coral cores. Custom equipment was constructed in the workshops at AIMS. Copper Refineries Pty. Ltd., Townsville, kindly provided copper sheet of very high purity. Helpful editorial comments and suggestions were provided by Dr. Robert Buddemeier and two anonymous reviewers. This is contribution no. 498 from the Australian Institute of Marine Science.

References

Buddemeier RW (1974) Environmental controls over annual and lunar monthly cycles in hermatypic coral calcification. Proc 2nd Int Coral Reef Symp 2:259–267

Buddemeier RW, Kinzie III RA (1975) The chronometric reliability of contemporary corals. In: Rosenberg GD, Runcorn SK (eds) Growth rhythms and the history of the earth's rotation. Wiley, London, pp 135–147

Buddemeier RW, Maragos JE, Knutson DW (1974) Radiographic studies of reef coral exoskeletons: ratios and patterns of coral growth. J Exp Mar Biol Ecol 14:179–200

Bureau of Radiological Health (1970) Mass attenuation coefficients. In: Radiological health handbook, rev edn. US Department of Health, Education and Welfare, Washington DC, pp 137–139

Burr AF (1978) Introduction to X-ray cross sections. In: Weast RC (ed) CRC handbook of chemistry and physics, 59th edn. CRC, West Palm Beach, pp E146–E150

Chalker B, Barnes D, Isdale P (1985) Calibration of X-ray densitometry for the measurement of coral skeletal density. Coral Reefs 4:95–100

Dodge RE, Brass GW (1984) Skeletal extension, density and calcification of the reef coral, *Montastrea annularis:* St. Croix, US Virgin Islands. Bull Mar Sci 34:288–307

Dodge RE, Thompson J (1974) The natural radiochemical and growth records in contemporary hermatypic corals from the Atlantic and Caribbean. Earth Planet Sci Lett 23:313–322

Dodge RE, Allen RC, Thompson J (1974) Coral growth related to resuspension of bottom sediments. Nature 247:574–577

Highsmith RC (1979) Coral growth rates and environmental control of density banding. J Exp Mar Biol Ecol 37:105–125

Hubbell JH (1969) Photon cross sections, attenuation coefficients, and energy absorption coefficients from 10 keV to 100 GeV. US Department of Commerce, National Bureau of Standards, Washington DC, pp 1–80

Hudson JH, Shinn EA, Halley RB, Lidz B (1976) Sclerochronology: a tool for interpreting past environments. Geology 4:361–364

Isdale P (1984) Fluorescent bands in massive corals record centuries of coastal rainfall. Nature 310:578–579

Knutson DW, Buddemeier RW (1973) Distribution of radionuclides in reef corals: opportunity for data retrieval and study of effects. In: Radioactive contamination of the marine environment. International Atomic Energy Agency, Vienna, pp 735–746

Knutson DW, Buddemeier RW, Smith SV (1972) Coral chronometers: seasonal growth bands in reef corals. Science 177:270–272

Moore WS, Krishnaswami S (1972) Coral growth rates using Ra-228 and Pb-210. Earth Planet Sci Lett 15:187–190

Moore WS, Krishnaswami S (1974) Correlation of X-radiographs revealed banding in corals with radiometric growth rates. Proc 2nd Int Coral Reef Symp 2:269–276

Moore WS, Krishnaswami S, Bhat SG (1973) Coral reef project – papers in memory of Dr. Thomas F. Goreau. 6. Radiometric determination of coral growth rates. Bull Mar Sci 23:157–176
Rhoads DC, Lutz RA (eds) (1980) Skeletal growth of aquatic organisms. Plenum, New York, pp 1–750
Veigele WJ (1973) Photon cross sections from 0.1 keV to 1 MeV for elements Z=1 to Z=94. Atomic Data 5:51–111
Wang Y (ed) (1969) Statistical aspects of nuclear counting. In: CRC handbook of radioactive nuclides. Chemical Rubber, Cleveland, pp 77–86
Wang CH, Willis DL (1965) Radiotracer methodology in biological science. Prentice-Hall, Englewood Cliffs, NJ, pp 1–382
Weber JN, White EW, Weber PH (1975) Correlation of density banding in reef coral skeletons with environmental parameters: the basis for interpretation of chronological records preserved in the coralla of corals. Paleobiology 1:137–149
Wellington GM, Glynn PW (1983) Environmental influences on skeletal banding in Eastern Pacific (Panama) corals. Coral Reefs 1:215–222

Appendix A

Photon beam attenuation

Radioisotope sources frequently emit photons at two or more energies. The attenuation at a beam of photons from this type of source requires a description which is more complex than Eq. (2). For, example if the source provides gamma photons at two distinct energies then

$$I = Io_1 \exp(-\mu_{m1} \varrho \chi) + Io_2 \exp(-\mu_{m2} \varrho \chi) , \quad (A1)$$

where Io_1 and Io_2 are the intensities of the two photon energies in the incident beam, and μ_{m1} and μ_{m2} are the mass absorption coefficients appropriate to those energies.

Equation (A1) provides that a plot of experimentally determined values of ln(I) versus the mass thickness of an absorbing material should initially approximate a straight line, then curve, and finally approximate a second straight line with a slope of lesser magnitude than that of the first line. The values of the parameters in equation (A1) can be determined by non-linear, least squares regression techniques.

While the four parameter model described by Eq. (A1) is an exact description of the attenuation of a gamma beam having two distinct energies, approximate solutions may be appropriate in certain circumstances. For example, if the lower energy photons are effectively absorbed by the minimum thickness of target material likely to be used then, at the limit $\mu m_1 \to \infty$ and $\exp(-\mu m_1 \varrho \chi) \to 0$, the first term of Eq. (A1) becomes, in effect, zero. The resultant equation is identical with Eq. (2) and is valid for all points except where the mass thickness approaches zero. A similar effect may be achieved by filtering the gamma beam with a metal target (typically a thin sheet of aluminium or copper) to remove substantially the low energy photons. In such circumstances Eq. (2) would apply to all experimental points.

Another situation in which an approximate solution is appropriate is where one of the two distinct energies is sufficiently high that the gamma photons pass through thicknesses of target material likely to be employed with minimal attenuation. A plot of experimentally determined values of ln(I) against mass thickness will then show a limited curvature; moreover, sufficient information will not be available to permit an accurate estimate of the mass absorption coefficient for the higher energy radiation (μm_2). In this situation, $\mu m_2 \to 0$, $\exp(-\mu m_2 \varrho \chi) \to 1$, and Eq. (A1) approximates to

$$I = Io_1 \exp(-\mu_{m1} \varrho \chi) + Io_2 . \quad (A2)$$

The overall contribution of the high energy count (Io_2) to the overall count may be determined by non-linear, least squares regression analysis or, alternatively, by using a filter which effectively absorbs all of the lower energy photons with little effect upon the high energy count. Equation (A2) can then be re-arranged to a linear form which is analogous to Eq. (3):

$$\ln(I - Io_2) = \ln(Io_1) - \mu_{m1} \varrho \chi . \quad (A3)$$

Over narrow experimental ranges of mass thickness and, particularly, when Io_2 is small in relation to Io_1, experimental plots of ln(I) against mass thickness may show no detectable curvature. In such cases, Eq. (A1) again approximates to Eq. (2).

If the radiation source provides photons at three distinct energies then

$$I = Io_1 \exp(-\mu m_1 \varrho \chi) + Io_2 \exp(-\mu m_2 \varrho \chi) + Io_3 \exp(-\mu m_3 \varrho \chi) . \quad (A4)$$

Since equations consistingof the sums of exponents are ill-conditioned, Eq. (A4) can also be used to simulate any situation in which the second term represents the dominant energy of a beam which includes one or more energies higher and lower than the dominant energy. Equation (A4) may, in practice, be simplified by the sorts of approximation already discussed. The ^{210}Pb source which is discussed emits energies such that both types of approximation may be appropriate.

In operational situations, attenuation is still basically exponential but is modified by two factors: geometry and buildup. These factors are reviewed by Hubbell (1969) who also provides extensive tabulations of attenuation coefficients. Geometry factors are a function of the relationship between the source and the detector. They arise because photon beams cannot be perfectly collimated. However, it is reasonably simple to make geometric factors insignificant by providing collimation which is effective over the actual source to detector distance.

Buildup results from the production of secondary photons in the absorber, usually by Compton scattering. A fraction of these will be scattered at such an angle that they enter the detector and are recorded. Thus buildup results in the detection of more events than would be expected based upon only the attenuation of the photon beam. Buildup can be countered very effectively by narrow and equal collimation of both the source and the detector. Very few scattered particles are then likely to remain within the beam limits provided by this collimation. Hence, secondary photons are not likely to contribute significantly to the count.

Appendix B

Sources and counting equipment

A block diagram of a gamma densitometry system is shown in Fig. B1. This communication examines the use of two such systems.

In the first system a low energy gamma emission, suitable for the determination of density in coral slabs, was provided by a 370 MBq (10 mCi) ^{210}Pb point source (capsule X.102, The radiochemical Centre, Amersham, UK). The active diameter of the source was 3 mm, and it was covered by a stainless steel end-window, 0.20–0.25 mm thick, to absorb ^{210}Bi alpha and beta particles and L X-rays. The photon energy of interest coming from the source was at 46.5 keV. Other, essentially interfering, emissions were Bi L X-rays of energies in the range 9.42–16.4 keV, Bremsstrahlung radiation extending to 1.16 MeV, and 800 keV gamma emissions from the ^{210}Po (The decay daughter and granddaughter of ^{210}Pb are ^{210}Bi and ^{210}Po, respectively).

The capsule containing the source was held at the centre of a solid brass shield of diameter 29.3 mm. The end-window of the capsule was directly beneath a brass-walled cap filled with lead. There was then 22.5 mm of lead covered by 1.0 mm of brass above the end-window of the source. Two such caps were constructed; one cap was

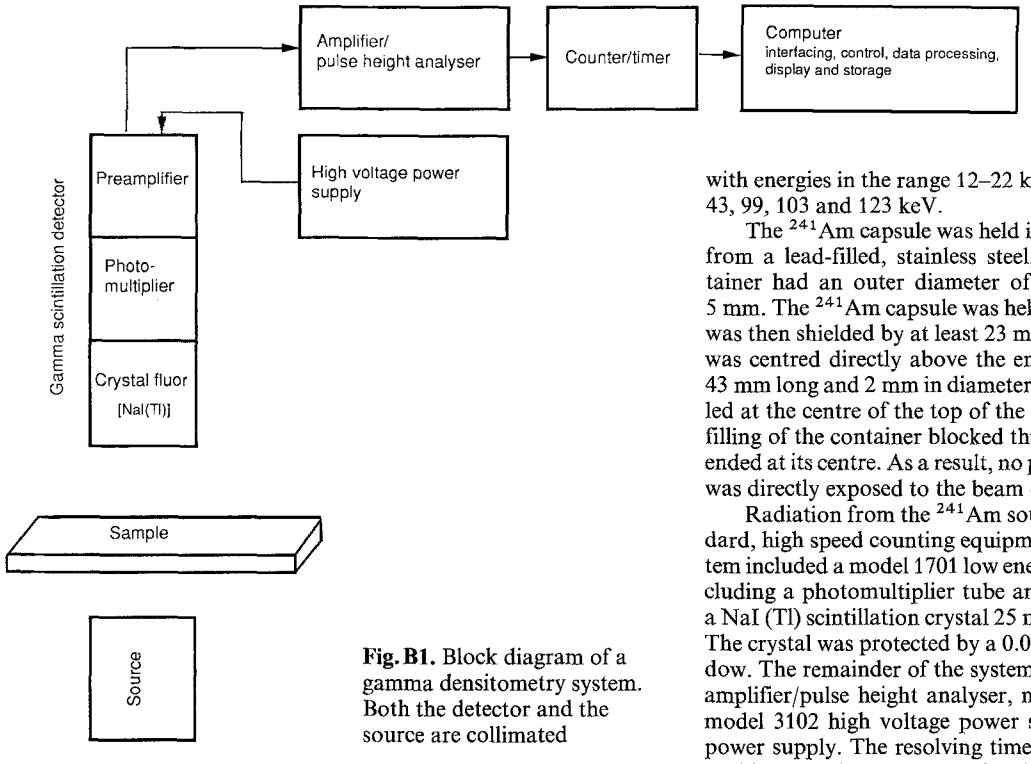

Fig. B1. Block diagram of a gamma densitometry system. Both the detector and the source are collimated

solid and the other cap had a 2 mm diameter hole drilled through it. This hole was positioned directly above the centre of the end-window of the source in order to provide a collimated beam of radiation at the outer surface of the cap.

A low energy gamma scintillation probe (LEG-1, Eberline Instrument Corporation, Santa Fe, NM, USA) was used to detect radiation from the ^{210}Pb source. The probe had a NaI(Tl) scintillation crystal 25.4 mm in diameter and 1.0 mm thick. The crystal was protected by a 0.025 mm thick aluminium end-window. The probe was connected to a Berthold LB 2040 radiation monitor (Berthold Laboratories, Wildbad, Federal Republic of Germany). Adjustments could be made to the photomultiplier voltage supplied from the radiation monitor to the probe. The monitor also had an adjustment for window position and an adjustment which allowed the window width to be varied symmetrically around the window position. An alternative monitor setting permitted the counting of gamma photons having energies in excess of a specified minimum value.

Count times were adjusted to provide total counts of 10000 or greater. The count rate was not allowed to exceed 60000 cpm because deadtime corrections were required when the count rate approached 80000 cpm.

In the second system, a low energy gamma emission suitable for the determination of density in coral slabs was provided by a 3.7 GBq (100 m Ci) ^{241}Am point source (capsule X.102, The Radiochemical Centre, Amersham, UK). The active diameter of the source was 3 mm, and it was covered by a stainless steel end-window, 0.20–0.25 mm thick. The photon energy of interest coming from the source was at 59.5 keV. Other emissions were Np L X-rays with energies in the range 12–22 keV and gamma photons at 26, 33, 43, 99, 103 and 123 keV.

The ^{241}Am capsule was held in a collimation castle constructed from a lead-filled, stainless steel, cylindrical container. The container had an outer diameter of 60 mm and a wall thickness of 5 mm. The ^{241}Am capsule was held at the centre of the cylinder and was then shielded by at least 23 mm of lead. The collimation tunnel was centred directly above the end-window of the capsule. It was 43 mm long and 2 mm in diameter. An 8 mm diameter hole was drilled at the centre of the top of the stainless steel container. The lead filling of the container blocked this hole and the collimation tunnel ended at its centre. As a result, no part of the stainless steel container was directly exposed to the beam of gamma photons.

Radiation from the ^{241}Am source was detected with NIM standard, high speed counting equipment (Canberra Packard). The system included a model 1701 low energy gamma scintillation probe including a photomultiplier tube and a preamplifier. The probe had a NaI (Tl) scintillation crystal 25 mm in diameter and 1.0 mm thick. The crystal was protected by a 0.025 mm thick aluminium end-window. The remainder of the system consisted of a model 1718 X-ray amplifier/pulse height analyser, model 2071A dual counter timer, model 3102 high voltage power supply, and model 2000 bin and power supply. The resolving time of the system is 200 ns, and this enables counting at a rate of 50000 counts/s with dead time error less than 1%.

At all settings for the radiation monitor, background rates were determined after the source had been removed. Data related to the calculation of mass attenuation coefficients were analysed after background subtraction.

For each counting system, the optimum photomultiplier voltage was determined by standard methods (Wang and Willis 1965). At fixed gain settings, graphs of count rate vs. photomultiplier voltage were constructed. The resultant curves showed a rapid rise in counter rate at low potentials, then a nearly flat plateau region of essentially constant counting rate as potentials were further increased, and, finally, a second region in which count rates increased rapidly with increasing potential. This second region of rising count rate is associated with thermal noise levels at the higher voltages. Such effects are known to be primarily responsible for the increase in total counting rate of the background observed towards the end of the plateau region of the curves. Accordingly, the scintillation detector was operated at a potential which was within the lower portion of the plateau.

Increase amplifier gain resulted in shortened plateau length, increased counting rate and decreased plateau slope. Since it is known that the effects on counting rate of photomultiplier potential and amplifier gain are similar, but that thermal noise is directly related to photomultiplier potential, increased amplifier gain was used, where available, to permit operation of the scintillation detector at a relatively low photomultiplier voltage. For the ^{210}Pb-Eberline-Bertold system the photomultiplier voltage was 1196V and the amplifier gain was factory preset. For the ^{241}Am-Canberra Packard system, the photomultiplier voltage was 1420V and the gain was 8.0.